

# Two-Dimensional Fluctuating Vesicles in Linear Shear Flow

Reimar Finken<sup>1a</sup>, Antonio Lamura<sup>2b</sup>, Udo Seifert<sup>1c</sup>, and Gerhard Gompper<sup>3d</sup>

<sup>1</sup> 2. Institut für Theoretische Physik, Pfaffenwaldring 57/III, Universität Stuttgart, 70550 Stuttgart, Germany

<sup>2</sup> Istituto Applicazioni Calcolo, Consiglio Nazionale delle Ricerche (CNR), Via Amendola 122/D, 70126 Bari, Italy

<sup>3</sup> Forschungszentrum Jülich GmbH, Institut für Festkörperforschung, 52425 Jülich, Germany

October 26, 2018

**Abstract.** The stochastic motion of a two-dimensional vesicle in linear shear flow is studied at finite temperature. In the limit of small deformations from a circle, Langevin-type equations of motion are derived, which are highly nonlinear due to the constraint of constant perimeter length. These equations are solved in the low temperature limit and using a mean field approach, in which the length constraint is satisfied only on average. The constraint imposes non-trivial correlations between the lowest deformation modes at low temperature. We also simulate a vesicle in a hydrodynamic solvent by using the multi-particle collision dynamics technique, both in the quasi-circular regime and for larger deformations, and compare the stationary deformation correlation functions and the time autocorrelation functions with theoretical predictions. Good agreement between theory and simulations is obtained.

**PACS.** 87.16.Dg Membranes, bilayers, and vesicles – 87.15.Ya Fluctuations – 67.40.Hf Hydrodynamics in specific geometries, flow in narrow channels

## 1 Introduction

The dynamics of soft objects such as drops, capsules and cells in flow represents a long-standing problem in science and engineering, but has received increasing interest recently, in particular due to its relevance to biological, medicinal and microfluidic applications. This problem is challenging from a theoretical point of view, because the shape of these objects is not given *a priori*, but determined dynamically from a balance of interfacial forces with fluid stresses. Improved experimental methods have revealed intriguing new dynamical shape transitions due to the presence of shear flow. The phenomenology of the dynamical behavior depends distinctively on the specific soft object immersed in the flow with fluid bilayer vesicles and elastic microcapsules as the most prominent classes.

Fluid bilayer vesicles assume a stationary tank-treading shape in linear shear flow, if there is no viscosity contrast between interior and exterior fluid [1]. If the interior fluid or the membrane becomes more viscous, a transition to a tumbling state can occur [2, 3, 4, 5, 6, 7]. Tank-treading was observed experimentally in infinite shear flow [8, 9] and for vesicles interacting with a rigid wall [10, 11], where a dynamic lift occurs [12, 13, 14, 15]. The tank-treading to tumbling transition was observed for the first time convincingly in an experiment only very recently [16]. In ad-

dition to the tank-treading to tumbling transition, an oscillating motion was predicted theoretically [17] and observed experimentally [16] and in simulations [18]. This type of motion has alternatively been called vacillating-breathing [17], swinging [18], or trembling [16, 19]. The theoretical description has been extended recently beyond first order in the shear rate [18, 19, 20].

At finite temperature, stochastic fluctuations of the membrane due to thermal motion affect the motion of the object. Due to the dissipative nature of the hydrodynamic interactions, vesicles in shear flow form a non-trivial model system for studying non-equilibrium stochastic dynamics. Since the effect of thermal noise on the transitions between the different modes of motion in general is a challenging task, in this paper we concentrate on the stochastic motion in the stationary tank-treading state. Our theoretical approach is similar to that of Ref. [21], where stochastic equations of motion were derived for quasi-spherical vesicles.

Most numerical methods solving the equation of motion of vesicles or capsules [1, 2] operate in the absence of thermal forces. An exception, which naturally includes thermal noise, is multi-particle collision dynamics (MPC), also known as stochastic rotation dynamics (SRD) [22, 23, 24, 25]. In this method, the fluid part is modeled on a particle rather than a continuum level. The microscopic equations of motion for the effective fluid are chosen to be evaluated efficiently on the one hand, and on the other hand to lead to the correct macroscopic hydrodynamics. This method has successfully been applied to flow around rigid objects [26, 27], polymers [28, 29] and

<sup>a</sup> e-mail: [finken@theo2.physik.uni-stuttgart.de](mailto:finken@theo2.physik.uni-stuttgart.de)

<sup>b</sup> e-mail: [a.lamura@ba.iac.cnr.it](mailto:a.lamura@ba.iac.cnr.it)

<sup>c</sup> e-mail: [useifert@theo2.physik.uni-stuttgart.de](mailto:useifert@theo2.physik.uni-stuttgart.de)

<sup>d</sup> e-mail: [g.gompper@fz-juelich.de](mailto:g.gompper@fz-juelich.de)

viscous vesicles [5, 6, 30, 18]. We employ the MPC simulation method to compare our theoretical predictions of correlation functions, inclination angles, and tank-treading frequencies with simulation data of vesicles. In order to obtain good statistics, we focus here on two-dimensional (2d) vesicles with a linear boundary.

The paper is organized as follows: After formulating the problem in section 2, we develop nonlinear stochastic equations of motion for quasi-circular vesicles in section 3. These are solved approximately using a mean field approach and a low temperature expansion in section 4. We also present the 2d version of the deterministic Keller-Skalak theory [31] in section 5, which takes into account the influence of the vesicle shape on the flow. The simulation method used is discussed in section 6. Finally we compare the calculations with simulation data in section 7 and discuss our results.

## 2 Problem formulation

We consider a model 2d vesicle immersed in a fluid of viscosity  $\eta_{\text{out}}$  with a 1d membrane boundary surrounding a fluid of viscosity  $\eta_{\text{in}}$  and at finite temperature  $T$ . Due to the incompressibility of the membrane and of the enclosed fluid, the area  $A_0$  and the length  $L_0$  of the membrane are constants. The membrane resists deformation with a bending rigidity  $\kappa$ , which is defined rigorously below in section 2.1. The fixed area defines a length scale

$$R_0 \equiv \sqrt{\frac{A_0}{\pi}}, \quad (1)$$

which can be used to define a number of dimensionless quantities. In the following, we use the excess length

$$\Delta \equiv \frac{L_0}{R_0} - 2\pi \quad (2)$$

and the dimensionless viscosity contrast

$$\lambda \equiv \frac{\eta_{\text{in}}}{\eta_{\text{out}}}. \quad (3)$$

Alternatively one can derive a length  $R^* \equiv L_0/(2\pi)$  from the length constraint, and use it to define a reduced area  $A^* \equiv A_0/(\pi R^{*2})$ . The reduced area is connected to the excess length by

$$A^* = \left(1 + \frac{\Delta}{2\pi}\right)^{-2}. \quad (4)$$

In a quiescent fluid, thermal stochastic forces acting on the membrane lead to a fluctuating shape, where the probability of any specific deformation can be calculated using the Boltzmann weight corresponding to the deformation energy  $\mathcal{H}[\mathbf{r}]$ . If an external flow field  $\mathbf{v}^\infty$  is switched on, the system ceases to be in equilibrium, and the statistical weight of a deformation cannot be calculated *a priori* using Boltzmann weights. We first derive the force balance governing the motion of a vesicle in stochastic Stokes flow, before we simplify the equations of motion in the limit of small deformations from a circular shape.

### 2.1 Constitutive equation of the membrane

We employ conventions of differential geometry following Ref. [32]. The shape of the vesicle is given by the shape function  $\mathbf{r}(s)$ , where  $0 \leq s \leq L$  denotes the arc length. The tangent vector  $\mathbf{t}(s) \equiv d\mathbf{r}(s)/ds$  is of unit length. The unit normal vector  $\mathbf{n}(s)$  is defined to point to the outside of the vesicle, and the orientation is chosen such that the pair  $(\mathbf{n}, \mathbf{t})$  forms a right handed system. The curvature  $k(s)$  is defined via the relation

$$d\mathbf{t}(s)/ds = -k(s)\mathbf{n}(s). \quad (5)$$

The 2d analog of the bending energy of a certain membrane deformation is given by the Helfrich term [33]

$$\mathcal{H}_\kappa[\mathbf{r}] \equiv \frac{\kappa}{2} \int_0^L ds k(s)^2, \quad (6)$$

which corresponds also to the bending energy of a semi-flexible polymer [34]. Note that for 3d vesicles, a spontaneous curvature  $C_0$  can appear in the bending energy for intrinsically asymmetric monolayers or asymmetric liquid environments. In 2d vesicles, we can ignore the spontaneous curvature, since it shifts the bending energy only by a topological constant, much like the Gaussian curvature contribution to the curvature energy can be ignored in 3d.

All deformations of the vesicle must preserve the length  $L$ . In addition, the fluid membrane is locally incompressible. This is ensured by introducing the tension  $\sigma(s)$  as a Lagrange parameter. The total energy thus reads

$$\mathcal{H}[\mathbf{r}] = \mathcal{H}_\kappa[\mathbf{r}] + \int_0^L ds \sigma(s). \quad (7)$$

From the Euler-Lagrange equations we can deduce the force acting on the membrane

$$\mathbf{f}^{\text{el}} = -\frac{\delta\mathcal{H}[\mathbf{r}]}{\delta\mathbf{r}} = \mathbf{t}(\sigma' + 2\kappa k k') + \mathbf{n}\left(\frac{\kappa}{2}k^3 - \kappa k'' - k\sigma\right). \quad (8)$$

Here the prime denotes a derivative with respect to the arc length  $s$ .

### 2.2 Stochastic Stokes flow

The elastic forces given by Eq. (8) are balanced by hydrodynamic forces mediated by the surrounding fluid. The motion of the fluid and the vesicle is only considered on time scales on which the fluid is incompressible, i.e.

$$\nabla \cdot \mathbf{v} = 0. \quad (9)$$

The length and time scales in typical experiments and simulations is such that the Reynolds number is very small. We only consider fluctuations on time scales on which the inertial term in the Navier-Stokes equation can be neglected. The velocity field  $\mathbf{v}$  of the fluid is then subject to the steady stochastic Stokes equation [35]

$$-\nabla p + \eta_\alpha \Delta \mathbf{v} + \nabla \cdot \mathbf{s} = 0, \quad (10)$$

where the thermal stress tensor  $\mathbf{s}(\mathbf{x})$  is assumed to be a Gaussian random variable with zero mean and correlations

$$\begin{aligned} \langle s_{ik} \rangle &= 0 \\ \langle s_{ik}(\mathbf{x}_1, t_1) s_{lm}(\mathbf{x}_2, t_2) \rangle &= 2k_B T \eta_\alpha \delta(\mathbf{x}_1 - \mathbf{x}_2) \delta(t_1 - t_2) \\ &\quad \times [\delta_{il} \delta_{km} + \delta_{im} \delta_{kl}]. \end{aligned} \quad (11)$$

Here  $\alpha \in \{\text{in}, \text{out}\}$  indicates the inner or outer fluid. Instead of calculating the stochastic velocity field of the flow, we only calculate the deterministic part of  $\mathbf{v}$ :

$$-\nabla p + \eta_\alpha \Delta \mathbf{v} = 0. \quad (12)$$

At the vesicle membrane we must have force balance between the deterministic and stochastic part of the hydrodynamic force and the elastic forces

$$\mathbf{f}^{\text{el}} + [\mathbf{T} \cdot \mathbf{n}]_{\text{in}}^{\text{out}} + \mathbf{s} \cdot \mathbf{n} = 0. \quad (13)$$

Here,  $\mathbf{T}$  denotes the deterministic hydrodynamic stress tensor with Cartesian components

$$T_{ik} \equiv -p \delta_{ik} + \eta_\alpha [\partial_i v_k + \partial_k v_i]. \quad (14)$$

Far away from the vesicle the velocity field assumes the externally given values

$$\mathbf{v}(\mathbf{x}) \rightarrow \mathbf{v}^\infty(\mathbf{x}), \quad |\mathbf{x}| \rightarrow \infty, \quad (15)$$

which is ensured by separating an induced part from the velocity field

$$\mathbf{v} \equiv \mathbf{v}^\infty + \mathbf{v}^{\text{ind}}, \quad (16)$$

and requiring that the induced part drops to zero far away from the vesicle. Assuming no-slip boundary conditions, the vesicle is advected by the flow, which implies

$$\partial_t \mathbf{r}(s, t) = \mathbf{v}(\mathbf{r}(s, t), t). \quad (17)$$

Here the dynamics still depends implicitly on  $\sigma(s)$ , which has to be chosen such that  $s$  remains the arc length, ensuring incompressibility. Eqs. (8,12–17) determine the stochastic motion of the vesicle.

### 3 Quasi-circular approximation

These equations can be simplified considerably if we restrict ourselves to vesicle shapes close to the circle. We parameterize the shapes as a function of the polar angle  $\phi$

$$\mathbf{r}(\phi) = R_0 \mathbf{e}_r(\phi) (1 + u(\phi)), \quad (18)$$

and consider small distortions  $u$ . The deformation amplitude  $u(\phi)$  is a real periodic function of  $\phi$  and can therefore be expanded into complex Fourier modes

$$u(\phi) \equiv \sum_{m=-\infty}^{\infty} u_m \frac{\exp(im\phi)}{\sqrt{2\pi}}. \quad (19)$$

For comparison with simulation data described below, an expansion into a real Fourier series is advantageous. We therefore also employ the expansion

$$u(\phi) \equiv a_0 + \sum_{m=1}^{\infty} a_m \cos(m\phi) + \sum_{m=1}^{\infty} b_m \sin(m\phi). \quad (20)$$

The real Fourier coefficients  $a_m, b_m$  are connected with the complex Fourier coefficients  $u_m$  via ( $m \neq 0$ )

$$u_m = \sqrt{\frac{\pi}{2}} (a_m - ib_m). \quad (21)$$

Area conservation fixes  $u_0$  in terms of the other  $u_m$

$$u_0 = -\frac{1}{\sqrt{8\pi}} \sum_{m \neq 0} |u_m|^2. \quad (22)$$

This relation will be used throughout the paper, and from now on sums over  $m$  exclude the  $m = 0$  term. The contour length  $L$  of the membrane is calculated to second order in  $u$  to be

$$L = 2\pi R_0 + \frac{R_0}{2} \sum_{m \neq 0} (m+1)(m-1) |u_m|^2. \quad (23)$$

Hence the excess length  $\Delta$  reads

$$\Delta = \frac{1}{2} \sum_{m \neq 0} (m^2 - 1) |u_m|^2. \quad (24)$$

Finally, the local curvature  $k$  evaluates to

$$R_0 k(\phi) = 1 - u''(\phi) = 1 + \sum_{m \neq 0} m^2 u_m \frac{\exp(im\phi)}{\sqrt{2\pi}}. \quad (25)$$

This leads to the bending energy (ignoring constant terms)

$$\mathcal{H}_\kappa = \frac{\kappa}{4R_0} \sum_{m \neq 0} (m^2 - 1) (m^2 - 3/2) |u_m|^2. \quad (26)$$

We now add the global length constraint (24) with a Lagrangian multiplier

$$\Sigma \equiv \kappa \sigma / R_0^2 \quad (27)$$

to the quadratic part of the bending energy. This leads to a quadratic expression for the total energy (88)

$$\mathcal{H} = \frac{\kappa}{2R_0} \sum_{m \neq 0} E_m(\sigma) |u_m|^2. \quad (28)$$

with

$$E_m(\sigma) \equiv (m+1)(m-1)[m^2 - 3/2 + \sigma]. \quad (29)$$

The bending forces (8) are determined by the deformation amplitudes  $u_m$  and by the instantaneous tension

$$\Sigma(\phi) \equiv \frac{\kappa}{R_0} \left( \sigma + \sum_{m \neq 0} \sigma_m \frac{\exp(im\phi)}{\sqrt{2\pi}} \right). \quad (30)$$

The homogeneous tension  $\kappa \sigma / R_0$  has already been included into the energy (28).

### 3.1 Velocity field

In polar coordinates, the general solution of Stokes' equation can be expanded into the fundamental modes [36]

$$\begin{aligned} \mathbf{v}_m^{\phi,\pm} &\equiv \nabla(r^{\pm|m|} \exp(im\phi))/\sqrt{2\pi}, \\ p_m^{\phi,\pm} &\equiv 0, \\ \mathbf{v}_m^{P,\pm} &\equiv \frac{1}{2(1\pm|m|)\sqrt{2\pi}} \left( \frac{|m|\pm 2}{2|m|} r^2 \nabla(r^{\pm|m|} \exp(im\phi)) \right. \\ &\quad \left. - \mathbf{r} r^{\pm|m|} \exp(im\phi) \right), \\ p_m^{P,\pm} &\equiv \eta_\alpha r^{\pm|m|} \exp(im\phi)/\sqrt{2\pi}. \end{aligned} \quad (31)$$

In this representation the cases  $|m| = 1$  and  $|m| = 0$  are special and have to be treated separately. They correspond to constant flow and rotational flow, respectively. The deeper reason why these are special cases is the Stokes paradox [36]. It follows from the boundary conditions that the induced velocity field on the inside must be composed of “+” modes, and of “-” modes on the outside.

The corresponding hydrodynamic stress tensor reads in  $(r, \phi)$  components

$$\begin{aligned} \mathbf{T}_m^{\phi,\pm} &= 2\eta r^{\pm|m|-2} \frac{\exp(im\phi)}{\sqrt{2\pi}} \\ &\quad \times \begin{pmatrix} |m|(|m| \mp 1) & im(\pm|m| - 1) \\ im(\pm|m| - 1) & -|m|(|m| \mp 1) \end{pmatrix} \end{aligned} \quad (32)$$

and

$$\mathbf{T}_m^{P,\pm} = \eta r^{\pm|m|} \frac{\exp(im\phi)}{2\sqrt{2\pi}} \begin{pmatrix} \pm|m| - 2 & im \\ im & \mp|m| - 2 \end{pmatrix}. \quad (33)$$

We can now express the 2d Oseen tensor in spectral components. The radial and polar components of the fluid velocity and hydrodynamic force at the reference circle are expanded into Fourier modes analogous to the expansion (19). The velocity field at the reference sphere together with the boundary conditions uniquely determines the expansion (31). From the spatial velocity field the hydrodynamic force  $\mathbf{f}^\pm \equiv \mathbf{T}^\pm \cdot \mathbf{n}$  can be calculated, leading to

$$\begin{pmatrix} f_m^{r,\text{ind}} \\ f_m^{\phi,\text{ind}} \end{pmatrix} = \frac{\eta_{\text{in}} + \eta_{\text{out}}}{R_0} \begin{pmatrix} 2|m| & 2i \text{sign}(m) \\ -2i \text{sign}(m) & 2|m| \end{pmatrix} \cdot \begin{pmatrix} v_m^{r,\text{ind}} \\ v_m^{\phi,\text{ind}} \end{pmatrix}. \quad (34)$$

### 3.2 External flow

In the absence of the vesicle the applied external flow must be regular everywhere. Therefore apart from constant flow and constant rotation only the “+” modes contribute in the expansion (31). To avoid the intricacies of the Stokes paradox, we neglect the possibility of constant flow. A general expansion of the external flow therefore reads

$$\mathbf{v}^\infty = \sum_m \Phi_m^\infty \mathbf{v}_m^{\phi,+} + P_m^\infty \mathbf{v}_m^{P,+} + \Omega r \mathbf{e}_\phi. \quad (35)$$

The last term in this expansion corresponds to rotational flow with the vorticity  $\Omega$ . For a finite viscosity contrast

there is a jump in the traction

$$\begin{aligned} \begin{pmatrix} f^{r,\infty} \\ f^{\phi,\infty} \end{pmatrix} &= \sum_m \frac{\exp(im\phi)}{\sqrt{2\pi}} (\eta_{\text{in}} - \eta_{\text{out}}) \\ &\quad \times \left[ \begin{pmatrix} 2|m|(|m| - 1) \\ 2im(|m| - 1) \end{pmatrix} \Phi_m^\infty + \begin{pmatrix} |m|/2 - 1 \\ im/2 \end{pmatrix} P_m^\infty \right] \end{aligned} \quad (36)$$

For the specific case of external linear shear flow

$$\begin{aligned} \mathbf{v}^\infty &= \dot{\gamma} y \mathbf{e}_x = (\dot{\gamma}/2)(y \mathbf{e}_x + x \mathbf{e}_y) - (\dot{\gamma}/2)(x \mathbf{e}_y - y \mathbf{e}_x) \\ &= -(i\dot{\gamma}\sqrt{2\pi}/8) \left[ \mathbf{v}_2^{\phi,+} - \mathbf{v}_{-2}^{\phi,+} \right] - (\dot{\gamma}/2) r \mathbf{e}_\phi, \end{aligned} \quad (37)$$

we can read off the only non-vanishing components

$$\begin{aligned} \Phi_2^\infty &= -\Phi_{-2}^\infty = -i\sqrt{2\pi}\dot{\gamma}/8, \\ \Omega &= -\dot{\gamma}/2. \end{aligned} \quad (38)$$

We will also use the dimensionless shear rate

$$\chi \equiv \dot{\gamma} \frac{\eta_{\text{out}} R_0^3}{\kappa} \quad (39)$$

and vorticity

$$\tilde{\Omega} \equiv \Omega \frac{\eta_{\text{out}} R_0^3}{\kappa} = -\frac{\chi}{2}. \quad (40)$$

### 3.3 Incompressibility condition

The flow at the vesicle membrane is subject to the incompressibility condition  $D_t \sqrt{g} = 0$ , which can be cast in the equivalent form  $\mathbf{t} \cdot \partial_\phi \mathbf{v}(\mathbf{r}(\phi)) = 0$ . To leading order in the deformation, this condition reads

$$v_r(R_0) + \partial_\phi v_\phi(R_0) = 0. \quad (41)$$

Separating the induced flow from the external flow, we have in Fourier components

$$\begin{aligned} v_m^{r,\text{ind}}(R_0) + im v_m^{\phi,\text{ind}}(R_0) &= -v_m^{r,\infty}(R_0) - im v_m^{r,\infty}(R_0) \\ &= |m|(|m| - 1) R_0^{|m|-1} \Phi_m^\infty + \frac{m^2}{4(|m| + 1)} P_m^\infty. \end{aligned} \quad (42)$$

Using this relation, we can eliminate  $v_m^{\phi,\text{ind}}$  and obtain

$$\begin{aligned} f_m^r &= 2 \frac{\eta_{\text{out}}}{R_0} (\lambda + 1) \frac{m^2 - 1}{|m|} v_m^{r,\text{ind}} \\ &\quad + \Phi_m^\infty 2(|m| - 1) \frac{\eta_{\text{out}}}{R_0} [ |m|(\lambda - 1) + (\lambda + 1) ] + P_m^\infty. \end{aligned} \quad (43)$$

### 3.4 Equation of motion

Neglecting the thermal fluctuating forces for the moment, we can derive a deterministic equation of motion. The force balance leads to

$$v_m^{\text{ind},r} = -(\kappa/\eta_{\text{out}}R_0^2)\Gamma_m E_m(\sigma)u_m + B_m\Phi_m^\infty R_0 \quad (44)$$

with

$$\Gamma_m \equiv \frac{|m|}{2(\lambda+1)(m^2-1)} \quad (45)$$

and

$$B_m \equiv -\frac{m^2(\lambda-1)+|m|(\lambda+1)}{(\lambda+1)(|m|+1)}. \quad (46)$$

From the induced velocity, we obtain the radial component of the full velocity field

$$v_m^r = v_m^{r,\text{ind}} + v_m^{r,\infty} = v_m^{r,\text{ind}} + |m|\Phi_m^\infty. \quad (47)$$

The advection equation then reads (cf. Ref. [21])

$$\partial_t u_m = i\Omega m u_m - (\kappa/\eta_{\text{out}}R_0^3)\Gamma_m E_m(\sigma)u_m + D_m\Phi_m^\infty \quad (48)$$

with

$$D_m \equiv \frac{2m}{\lambda+1} \quad (49)$$

At non-zero temperature, thermal forces must be taken into account in the force balance. The deterministic equation of motion (48) then becomes a Langevin equation

$$\partial_t u_m = i\Omega m u_m - (\kappa/\eta_{\text{out}}R_0^3)\Gamma_m E_m(\sigma)u_m + D_m\Phi_m^\infty + \zeta_m. \quad (50)$$

The form of the thermal noise  $\zeta_m$  can be obtained directly from the noise term in Eq. (13). It is much easier, however, to determine  $\zeta_m$  from the Einstein relation, which must be valid in equilibrium. We assume that the equilibrium noise is valid also for non-vanishing shear flow and choose

$$\langle \zeta_m(t)\zeta_{m'}(t') \rangle = 2(k_B T \Gamma_m / \eta_{\text{out}} R_0^3) \delta_{m,-m'} \delta(t-t'). \quad (51)$$

Eq. (50) is the correct stochastic equation of motion for the vesicle deformation modes  $u_m$ . The tension  $\sigma$  is at each instance determined such that the length constraint (24) is fulfilled. Taking the time derivative of Eq. (24) and using Eq. (50), we can solve for the tension

$$\sigma = \left[ \sum_{m \neq 0} (m^2 - 1)^2 \Gamma_m |u_m|^2 \right]^{-1} \sum_{m \neq 0} (m^2 - 1) \left[ i\Omega m |u_m|^2 - \frac{\kappa}{\eta_{\text{out}} R_0^3} \Gamma_m E_m(0) |u_m|^2 + D_m u_m^* \Phi_m^\infty + u_m^* \zeta_m \right]. \quad (52)$$

When this expression is inserted back into Eq. (50), the resulting noise term becomes dependent on the instantaneous values of the  $u_m$ . While such non-linear noise terms hold interesting physics, we first concentrate on tractable approximate solutions to the stochastic equation of motion.

## 4 Approximate solutions

### 4.1 Mean-field treatment

At finite temperature, higher-order modes are excited by stochastic thermal forces and therefore cannot be neglected. The full non-linear set of Langevin equations (50) in combination with the expression (52) for  $\sigma$  is too complex to admit a general solution. We can, however, gain further insight in the tank-treading regime using a mean-field description. We replace the fluctuating tension  $\sigma$  in Eq. (50) by a constant, which has to be determined self-consistently from the length constraint. The Langevin equations (50) then become linear and decouple. In the stationary state, only the  $m = 2$  deformations have a finite mean,

$$\langle u_2 \rangle = \frac{\eta_{\text{out}} R_0^3}{\kappa} \frac{D_2}{\Gamma_2 E_2(\sigma) + i\chi} \Phi_2^\infty. \quad (53)$$

On average, the vesicle is elliptical. As a measure of the deformation from the circle we define the Taylor deformation parameter

$$D \equiv \frac{L - S}{L + S}, \quad (54)$$

where  $L$  and  $S$  denote the long and short axis of the ellipse. In the mean-field treatment we have

$$D = \frac{2}{3} \frac{\chi}{[(5/2 + \sigma)^2 + 9\chi^2(1 + \lambda)^2]^{1/2}}. \quad (55)$$

The inclination angle is obtained from Eq. (53)

$$\Theta = \frac{1}{2} \arctan \frac{5/2 + \sigma}{\chi(1 + \lambda)}. \quad (56)$$

The deviations from the mean

$$\delta u_m \equiv u_m - \langle u_m \rangle \quad (57)$$

obey the homogeneous Langevin equation

$$\partial_t \delta u_m = im\Omega \delta u_m - (\kappa/\eta_{\text{out}}R_0^3)\Gamma_m E_m(\sigma)\delta u_m + \zeta_m. \quad (58)$$

The stationary noise correlations are best evaluated using a time Fourier transform

$$\widehat{\delta u}(\omega) \equiv \int dt \exp(-i\omega t) \delta u(t), \quad (59)$$

leading to

$$i\omega \widehat{\delta u}_m = -im\Omega \widehat{\delta u}_m - (\kappa/\eta_{\text{out}}R_0^3)\Gamma_m E_m(\sigma)\widehat{\delta u}_m + \widehat{\zeta}_m \quad (60)$$

We can solve for  $\widehat{\delta u}_m(\omega)$  and obtain the correlations

$$\langle \widehat{\delta u}_m(\omega) \widehat{\delta u}_{-m}(-\omega) \rangle = \frac{2k_B T \Gamma_m / \eta_{\text{out}} R_0^2}{(\omega + m\Omega)^2 + \left[ \frac{\kappa \Gamma_m E_m}{\eta_{\text{out}} R_0^3} \right]^2}. \quad (61)$$

We have left the  $\sigma$ -dependence of  $E_m$  implicit for clarity. The time correlation function becomes ( $\Delta t > 0$ )

$$\begin{aligned} \langle \delta u_m(0) \delta u_{-m}(\Delta t) \rangle &= \int \frac{d\omega}{2\pi} \exp(i\omega \Delta t) \langle \widehat{\delta u}_m(\omega) \widehat{\delta u}_{-m}(-\omega) \rangle \\ &= \frac{k_B T R_0}{\kappa E_m} \\ &\quad \times \exp \left[ - \left( \frac{\kappa \Gamma_m E_m}{\eta_{\text{out}} R_0^3} + im\Omega \right) \Delta t \right]. \end{aligned} \quad (62)$$

with the stationary equal-time correlations

$$\langle \delta u_m(t) \delta u_{-m}(t) \rangle = \frac{k_B T R_0}{\kappa E_m(\sigma)}. \quad (63)$$

The amplitudes  $u_m$  with different  $m$  are uncorrelated at all times. Comparison with simulation data is easier using the real Fourier coefficients (20). The corresponding correlation functions read

$$\begin{aligned} \langle \delta a_m(0) \delta a_m(t) \rangle &= \langle b_m(0) b_m(t) \rangle \\ &= \frac{k_B T R_0}{\pi \kappa E_m} \exp \left( - \frac{\kappa \Gamma_m E_m}{\eta_{\text{out}} R_0^3} t \right) \cos(m\dot{\gamma}t/2), \\ \langle \delta a_m(0) \delta b_m(t) \rangle &= -\langle b_m(0) a_m(t) \rangle \\ &= \frac{k_B T R_0}{\pi \kappa E_m} \exp \left( - \frac{\kappa \Gamma_m E_m}{\eta_{\text{out}} R_0^3} t \right) \sin(m\dot{\gamma}t/2), \end{aligned} \quad (64)$$

and

$$\begin{aligned} \langle \delta a_m(0) \delta a_m(0) \rangle &= \langle \delta b_m(0) \delta b_m(0) \rangle = \frac{k_B T R_0}{\pi \kappa E_m(\sigma)} \\ \langle \delta a_m(0) \delta b_m(0) \rangle &= 0 \end{aligned} \quad (65)$$

The fluctuating  $u_m$  contribute to the excess length according to Eq. (24). Although the length constraint cannot be obeyed exactly with a constant tension, we determine  $\sigma$  such that the constraint (24) is fulfilled on average. The total excess length has a systematic and a fluctuating part

$$\Delta = \bar{\Delta}(\sigma) + \sum_{m \geq 2} \Delta_m(\sigma), \quad (66)$$

with

$$\begin{aligned} \bar{\Delta}(\sigma) &\equiv \sum_{m > 0} (m^2 - 1) \frac{D_m^2 |\Phi_m^\infty|^2}{\Gamma_m^2 E_m(\sigma)^2 + m^2 \tilde{\Omega}^2} \\ &= \frac{3\pi}{2} \frac{\chi^2}{(5/2 + \sigma)^2 + \chi^2(1 + \lambda)^2}. \end{aligned} \quad (67)$$

and

$$\Delta_m(\sigma) \equiv (m^2 - 1) \langle |\delta u_m|^2 \rangle = \frac{k_B T R_0}{\kappa(m^2 - 3/2 + \sigma)} \quad (68)$$

Thus  $\sigma$  is determined implicitly by the solution of Eq. (66). For future reference, we note that the contribution of the

fluctuating parts to the excess length can be determined analytically to be

$$\begin{aligned} \sum_{m \geq 2} \Delta_m(\sigma) &= \frac{k_B T R_0}{\kappa \sqrt{2} (4\sigma^2 - 8\sigma + 3)} \left[ \sqrt{2}(7 - 6\sigma) \right. \\ &\quad \left. + \pi \sqrt{3 - 2\sigma} (2\sigma - 1) \cot \left( \pi \sqrt{3/2 - \sigma} \right) \right]. \end{aligned} \quad (69)$$

While this expression is exact, its behavior as a function of  $\sigma$  is not obvious (for example, the ‘‘singularities’’ at  $\sigma = 1/2$  and  $\sigma = 3/2$  are only apparent). We therefore give the leading asymptotic behavior

$$\sum_{m \geq 2} \Delta_m(\sigma) \approx \frac{k_B T R_0}{\kappa} \begin{cases} 1/(\sigma + 5/2) + 25/48 & \sigma \rightarrow -5/2 \\ \pi(4\sigma)^{-1/2} & \sigma \rightarrow \infty. \end{cases} \quad (70)$$

## 4.2 Zero temperature

At large shear rates, nearly the entire excess length is stored in the systematic part  $\bar{\Delta}$ . As a crossover shear rate  $\chi_c$ , we can define the shear rate at which the two contributions in condition (66) become equal

$$\bar{\Delta}(\sigma, \chi_c) \equiv \sum_{m \geq 2} \Delta_m(\sigma) = \frac{\Delta}{2}. \quad (71)$$

This set of equations must be solved numerically for each  $\Delta$ . In the limit  $\chi \gg \chi_c$  we can ignore the thermal forces. In this case, the equation of motion (50) becomes the deterministic Eq. (48), and the tension is determined by Eq. (52) with  $\zeta_m = 0$ .

We can easily obtain the stationary state from  $\partial_t u_m^0 = 0$ , i.e.

$$u_m^0 = \frac{\eta_{\text{out}} R_0^3}{\kappa} \frac{D_m}{\Gamma_m E_m(\sigma_0) + im\tilde{\Omega}} \Phi_m^\infty. \quad (72)$$

The homogeneous tension  $\sigma_0$  is determined from the length constraint (24). In the case of constant linear shear flow, only the  $m = \pm 2$  components are non-zero and are equal in magnitude. The length constraint thus reads  $|u_{\pm 2}| = (\Delta/3)^{1/2}$ , or

$$\begin{aligned} \Delta &= 3 \frac{D_2^2}{\Gamma_2^2 E_2^2 + 4\tilde{\Omega}^2} \frac{2\pi\chi^2}{64} \\ &= \frac{3\pi}{2(1 + \lambda)^2} \frac{\chi^2}{(5/2 + \sigma_0)^2 / (9(1 + \lambda))^2 + \chi^2}. \end{aligned} \quad (73)$$

The homogeneous tension in the stationary state is thus given by

$$\sigma_0 = -5/2 + 3\chi(1 + \lambda) \left[ \frac{3\pi}{2\Delta(1 + \lambda)^2} - 1 \right]^{1/2}. \quad (74)$$

$E_2$  vanishes at a critical viscosity ratio

$$\lambda_c = \sqrt{\frac{3\pi}{2\Delta}} - 1. \quad (75)$$

This corresponds to a tank-treading to tumbling transition, as can be seen when we allow for time-dependent  $\sigma_0$ : In linear shear flow, only the  $m = 2$  modes are excited. In the long time limit we can therefore assume that all other modes have decayed. In analogy with the 3d treatment [17], we can write  $u_2$  in polar form

$$u_2 \equiv (\Delta/3)^{1/2} \exp(-2i\Theta), \quad (76)$$

where  $\Theta$  is the inclination angle of the vesicle with respect to the shear direction. Taking the real and imaginary part of Eq. (48) gives the familiar Jeffery's equation [37]

$$\dot{\Theta} = \dot{\gamma} \left[ -\frac{1}{2} + \frac{1}{2} \frac{\sqrt{3\pi}}{(\lambda+1)\sqrt{2\Delta}} \cos(2\Theta) \right]. \quad (77)$$

For  $\lambda < \lambda_c$ , Eq. (77) admits two stationary solutions, of which only the positive is linearly stable

$$\Theta_0 \equiv \frac{1}{2} \arccos \left( \frac{(\lambda+1)^2 2\Delta}{3\pi} \right)^{1/2}. \quad (78)$$

This corresponds to stationary tank-treading motion, where the tank-treading frequency at zeroth order is given by the external flow

$$\omega_{tt}^{\text{QC}} \equiv \frac{\dot{\gamma}}{2}. \quad (79)$$

For  $\lambda > \lambda_c$ , the right hand side of Eq. (77) is always negative, and the vesicle starts to tumble. In two dimensions, no analogy to a swinging motion (cf. Refs. [17, 16, 18, 19]) exists, since the volume and length constraint already uniquely determine the shape of an ellipse.

### 4.3 First-order correction to the large shear-rate limit

In the mean-field approach the tension  $\sigma$  is assumed constant and all modes fluctuate independently with amplitudes given by Eq. (63). In this picture, the length constraint is not fulfilled rigorously but only on average. For strictly enforced length constraint the tension must fluctuate according to Eq. (52), which induces correlations between the deformation amplitudes. While this general effect is worth considering in its own right, here we concentrate on the much simpler large shear rate (or low temperature) limit as a perturbation of the deterministic solution.

At  $T = 0$ , the whole excess length  $\Delta$  is stored in the  $|m| = 2$  mode. Perturbing the modulus of the amplitude  $|u_2|$  alters the excess length  $\Delta$  to first order and is prohibited by the constraint (2). Perturbing the other modes alters  $\Delta$  only to second order. At low temperature, we can therefore assume the polar decomposition (76). Taking the real and imaginary part of the equation of motion (50), we arrive at a Langevin equation for the inclination angle

$$\dot{\Theta} = \dot{\gamma} \left[ -\frac{1}{2} + \frac{1}{2} \frac{\sqrt{3\pi}}{(\lambda+1)\sqrt{2\Delta}} \cos(2\Theta) \right] + \xi, \quad (80)$$

where the noise term

$$\xi \equiv \sqrt{\frac{3}{4\Delta}} \text{Im}[\zeta_2 \exp(2i\Theta)] \quad (81)$$

is Gaussian and delta-correlated

$$\langle \xi(t)\xi(0) \rangle = \frac{3}{4\Delta} \Gamma_2 k_B T \delta(t). \quad (82)$$

In the stationary regime  $\Theta$  fluctuates around the mean value

$$\Theta \equiv \Theta_0 + \Delta\Theta, \quad (83)$$

where  $\Theta_0$  is given by Eq. (78). For small  $\Delta\Theta$  we can expand Eq. (80) to obtain

$$\Delta\dot{\Theta} = -\dot{\gamma} \sqrt{\frac{2\pi}{3\Delta}} \frac{1}{\lambda+1} \sin(2\Theta_0) \Delta\Theta + \xi. \quad (84)$$

This implies the stationary correlations

$$\langle \Delta\Theta^2 \rangle = \frac{R_0 k_B T}{\kappa \chi \Delta^{1/2}} \frac{1}{8} \left[ \frac{3\pi}{2} - (\lambda+1)^2 \Delta \right]^{-1/2} = \frac{3k_B T R_0}{8\kappa \Delta E_2(\sigma_0)}, \quad (85)$$

where we have used Eq. (78). For small  $\Delta$  we read off

$$\langle \Delta\Theta^2 \rangle^{1/2} \approx \left( \frac{1}{129\pi} \right)^{1/4} \left( \frac{\kappa \chi \Delta^{1/2}}{R_0 k_B T} \right)^{-1/2} \approx 0.20 \left( \frac{\kappa \chi \Delta^{1/2}}{R_0 k_B T} \right)^{-1/2}. \quad (86)$$

Finally, we calculate the fluctuations of the Fourier modes  $a_2, b_2$ . The polar expansion (76) implies

$$\begin{aligned} a_2 &= \sqrt{\frac{2\Delta}{3\pi}} \cos(2\Theta), \\ b_2 &= \sqrt{\frac{2\Delta}{3\pi}} \sin(2\Theta). \end{aligned} \quad (87)$$

We derive the correlation functions of the  $m = 2$  modes from Eq. (85) to be

$$\begin{aligned} \langle \delta a_2 \delta a_2 \rangle &= \frac{k_B T R_0}{\pi \kappa E_2(\sigma_0)} \cos^2(2\Theta_0), \\ \langle \delta a_2 \delta b_2 \rangle &= \frac{k_B T R_0}{\pi \kappa E_2(\sigma_0)} \cos(2\Theta_0) \sin(2\Theta_0), \\ \langle \delta b_2 \delta b_2 \rangle &= \frac{k_B T R_0}{\pi \kappa E_2(\sigma_0)} \sin^2(2\Theta_0). \end{aligned} \quad (88)$$

## 5 Keller-Skalak theory

In the theory of Keller and Skalak [31], a three-dimensional vesicle is assumed to have a fixed ellipsoidal shape

$$(x_1/a_1)^2 + (x_2/a_2)^2 + (x_3/a_3)^2 = 1, \quad (89)$$

where the  $a_i$  are the semi-axes of the ellipsoid, and the coordinate axes  $x_i$  point along its principal directions. The  $x_1$  and  $x_2$  axes, with  $a_1 > a_2$ , are chosen to lie in the  $xy$  plane and are rotated through an angle  $\Theta$  with respect

to the  $x$  and  $y$  axes. The components of the undisturbed shear flow are  $(\dot{\gamma}y, 0, 0)$ . The velocity field at the membrane is assumed to be

$$\mathbf{v} = \omega_{tt}^{\text{KS}} (-a_1/a_2)x_2, (a_2/a_1)x_1, 0, \quad (90)$$

where  $\omega_{tt}^{\text{KS}}$  is a parameter having the dimensions of a frequency. The energy supplied by the external flow has to be balanced with the energy dissipated inside the vesicle. The motion of the vesicle derived from this energy balance reads [31]

$$\frac{d\Theta}{dt} = -\frac{\dot{\gamma}}{2} + B \cos(2\Theta), \quad (91)$$

with

$$B = \frac{\dot{\gamma}}{1+r_2^2} \left\{ \frac{(1-r_2^2)^2 [z_2(1-\lambda) - 2] - 8r_2^2}{2(1-r_2^2)[z_2(1-\lambda) - 2]} \right\} \quad (92)$$

and

$$\omega_{tt}^{\text{KS}} = 2\dot{\gamma} \frac{r_2(1+r_2^2)}{(1-r_2^2)^2 [z_2(1-\lambda) - 2] - 8r_2^2}. \quad (93)$$

The factors appearing in Eqs. (91)-(93) are given by

$$\begin{aligned} r_2 &\equiv a_2/a_1, & r_3 &\equiv a_3/a_1, & z_2 &\equiv g_3'(\alpha_1^2 + \alpha_2^2), \\ \alpha_1 &\equiv r_2^{-1/3} r_3^{-1/3}, & \alpha_2 &\equiv r_2^{2/3} r_3^{-1/3}, & \alpha_3 &\equiv r_2^{-1/3} r_3^{2/3}, \end{aligned} \quad (94)$$

and

$$g_3' \equiv \int_0^\infty (\alpha_1^2 + s)^{-3/2} (\alpha_2^2 + s)^{-3/2} (\alpha_3^2 + s)^{-1/2} ds. \quad (95)$$

For  $B > \dot{\gamma}/2$ , we obtain a steady tank-treading angle

$$\Theta = \frac{1}{2} \arccos \left( \frac{\dot{\gamma}}{2B} \right). \quad (96)$$

We calculate the inclination angle  $\Theta$  and the tank-trading frequency  $\omega_{tt}^{\text{KS}}$  by adapting the Keller-Skalak theory to two dimensions. We numerically solve Eqs. (91)-(93) in the limit  $r_3 \rightarrow +\infty$  keeping  $r_2$  finite, which formally corresponds to an ellipsoid with an infinite semi-axis in the  $z$  direction.

## 6 Simulation method

A 2d vesicle model system was simulated using the multi-particle collision (MPC) dynamics [22, 5, 25]. In this method the fluid is not treated on a continuum level, but rather by a stochastic dynamics of effective fluid particles.

### 6.1 Solvent dynamics

We consider a two-dimensional system made of  $N_s$  identical particles of mass  $m_s$  whose positions  $\mathbf{r}_i(t)$  and velocities  $\mathbf{v}_i(t)$ ,  $i = 1, 2, \dots, N_s$ , are continuous variables. The time is discretized in intervals  $\Delta t_s$ . The evolution occurs

in two consecutive steps, streaming and collision. In the streaming step, particles move ballistically,

$$\mathbf{r}_i(t + \Delta t_s) = \mathbf{r}_i(t) + \mathbf{v}_i(t) \Delta t_s. \quad (97)$$

For the collision step, the system is divided into the cells of a regular square lattice of mesh size  $a$ . Each of these cells is the interaction area where an instantaneous multi-particle collision occurs, which changes particles velocities as [22]

$$\mathbf{v}_i(t + \Delta t_s) = \mathbf{u}(t) + \Omega[\mathbf{v}_i(t) - \mathbf{u}(t)], \quad (98)$$

where  $\mathbf{u}$  is the average velocity of the colliding particles in a cell. The velocity field  $\mathbf{u}$  is considered to be the macroscopic velocity of the fluid and it is assumed to have the coordinates of the center of the cell.  $\Omega$  denotes a stochastic rotation matrix which rotates, with equal probability, by an angle of either  $+\alpha$  or  $-\alpha$ . The collisions are performed simultaneously on all the particles in a cell with the same rotation  $\Omega$ , but  $\Omega$  may differ from cell to cell. The local momentum and kinetic energy are conserved under this dynamics. The kinetic energy of particles fixes the temperature  $k_B T$ , where  $k_B$  is the Boltzmann constant, via the equipartition theorem.

It was shown in Ref. [38] that a proper description of hydrodynamics in MPC requires large Schmidt numbers. This can be accomplished by choosing a mean-free path  $l = \Delta t_s \sqrt{k_B T / m_s}$ , which is small compared to the cell size  $a$ . It is known that a value of  $l$  much smaller than  $a$  breaks the Galilean invariance [39] and that this problem can be solved by applying a random shift procedure [39]. The viscosity of the solvent fluid is [24, 40]

$$\begin{aligned} \eta = & \left[ \frac{l}{2a} \left[ \frac{n_c^2}{(n_c - 1 + e^{-n_c}) \sin^2 \alpha} - n_c \right] \right. \\ & \left. + \frac{a}{12l} (n_c - 1 + e^{-n_c}) (1 - \cos \alpha) \right] \frac{\sqrt{m_s k_B T}}{a}, \end{aligned} \quad (99)$$

with particle density  $\rho = n_c m_s / a^2$  and number  $n_c$  of particles per cell.

In order to enforce shear flow, we place our system of size  $L_x \times L_y$  between two horizontal walls. The upper and the lower walls slide along the  $x$  direction with velocities  $\mathbf{v}_{wall} = (v_{wall}, 0)$  and  $-\mathbf{v}_{wall}$ , respectively, with  $v_{wall} > 0$ . Periodic boundary conditions are used along the  $x$  direction. Along the  $y$  direction, we use a modified bounce-back boundary condition which consists in requiring that particles hitting the walls change their velocities according to  $\mathbf{v}_i \rightarrow 2\mathbf{v}_{wall} - \mathbf{v}_i$ . Together with virtual particles in partly filled cells at walls, this describes no-slip boundary conditions very well [26, 27]. A linear flow profile  $(u_x, u_y) = (\dot{\gamma}y, 0)$  is obtained with shear rate  $\dot{\gamma} = 2v_{wall}/L_y$ , with the walls placed at  $y = \pm L_y/2$ . The relative velocities in the collision cells are rescaled after each time step  $\Delta t_s$  in order to keep the temperature constant in the (driven) system.

### 6.2 Membrane model

The vesicle membrane is modeled by connecting  $N_p$  beads of mass  $m_p$  successively with bonds into a closed ring.



Neighboring beads along the closed chain are connected to each other with the harmonic potential

$$U_{\text{bond}} \equiv \frac{k_h}{2} \sum_{i=1}^{N_p} \frac{(|\mathbf{r}_i - \mathbf{r}_{i-1}| - r_0)^2}{r_0^2}, \quad (100)$$

where  $k_h$  is a spring constant,  $\mathbf{r}_i$  is the position vector of the  $i$ -th bead, and  $r_0$  is the average bond length. The bending energy (26) is modeled on the discrete level by a bending potential

$$U_{\text{bend}} \equiv \frac{\kappa}{r_0} \sum_{i=1}^{N_p} (1 - \cos \beta_i), \quad (101)$$

where  $\beta_i$  is the angle between successive bonds. The fluid modeled with the MPC method is compressible. To enforce the area constraint in the presence of thermal and hydrodynamic forces, we add a constraint potential

$$U_{\text{area}} \equiv \frac{k_A}{2} \frac{(A - A_0)^2}{r_0^4}. \quad (102)$$

### 6.3 Coupling of membrane and solvent dynamics

The membrane-solvent interaction must prevent solvent particles from crossing the membrane and enforce no-slip boundary conditions on the membrane. Therefore we place hard disks centered on the membrane beads. The disk radius  $r_p$  is set in order to ensure overlapping of disks and a complete coverage of the membrane. The exchange of momentum between the solvent particles and the membrane occurs in the following way. After updating bead positions and velocities via molecular dynamics (MD), we freely stream all the solvent particles. We then execute bounce-back scattering between solvent and membrane disks only when a solvent particle  $j$  and a disk  $i$  satisfy the conditions  $|\mathbf{r}_i - \mathbf{r}_j| < r_p$  and  $(\mathbf{r}_i - \mathbf{r}_j) \cdot (\mathbf{v}_i - \mathbf{v}_j) < 0$ . This means that if the two collision partners  $i$  and  $j$  overlap and move towards each other, then their velocities are updated according to

$$\begin{aligned} \mathbf{v}_i &\rightarrow \mathbf{v}_i - 2 \frac{m_s}{m_s + m_p} (\mathbf{v}_i - \mathbf{v}_j), \\ \mathbf{v}_j &\rightarrow \mathbf{v}_j + 2 \frac{m_p}{m_s + m_p} (\mathbf{v}_i - \mathbf{v}_j). \end{aligned} \quad (103)$$

To avoid that a solvent particle moves too far inside a disk, we require that  $l \ll r_p$ . The collision step (98) is performed only on those solvent particles which did not scatter. If the collision step were executed also on the scattered solvent particles, they might continue to collide with the same disk in the next time step. The fluids in the interior and exterior of the vesicle are taken to be the same, in particular to have the same viscosity.

A chain of disks of finite radius  $r_p$  has an inner length available to the solvent particles which is smaller than the outer length. Since the solvent has the same density inside and outside, the outer fluid exerts a compression force on

the membrane until the inner density increases so that an expansion force compensates the compression one. It is straightforward to show [6] that the density increase is  $\Delta\rho/\rho = 2r_p/R^*$  where  $2r_p$  is the effective membrane thickness. This requires that  $R_0$  is large enough compared to the disk radius  $r_p$  to reduce such compression effects. The number of solvent particles placed inside the vesicle fixes an average area. However, since the MPC fluid is compressible, shear and bending rigidity effects may change the area  $A$ . For this reason the constraint potential (102) is introduced to keep the area constant.

### 6.4 Parameters

In experiments with vesicles in shear flow, inertial effects are negligible since the Reynolds number  $Re \equiv \dot{\gamma}\rho R^{*2}/\eta_{\text{out}}$  is very small. We express our results using the reduced area  $A^* = A_0/\pi R^{*2}$ , defined in Eq. (4), and the reduced shear rate  $\chi = \dot{\gamma}\eta_{\text{out}}R_0^3/\kappa$ , see Eq. (39), as relevant dimensionless quantities.

We set  $\alpha = \pi/4$ ,  $n_c = 10$ , and  $l = 0.008a$ . This implies a viscosity  $\eta_{\text{out}} = \eta_{\text{in}} \simeq 28.0\sqrt{m_s k_B T}/a$ . We use  $L_x = 150a$ ,  $L_y = 90a$ ,  $R^* = 15.3a$ , and  $v_{\text{wall}}$  such that  $Re < 0.1$  for all the cases we considered with  $0.5 \leq \chi \leq 10.0$ . Finally, we set  $m_p = 10m_s$ ,  $N_p = 96$ ,  $\Delta t_p = \Delta t_s/20$ ,  $r_p = 0.9a$ ,  $r_0 = a$ ,  $\kappa = 40k_B T a$ ,  $k_A = 0.5k_B T$ ,  $k_h = 4000k_B T$ . The area  $A_0$  is chosen in such a way that  $0.7 \leq A^* \leq 0.95$ . With the choices for  $k_A$  and  $k_h$  the area and the length of the vesicle are kept constant with a deviation of less than 1% of the target values for all simulated systems. A snapshot of a simulated vesicle and the resulting velocity field for the reduced area  $A^* = 0.95$  and reduced shear rate  $\chi = 5.6$  is shown in Fig. 1.

## 7 Results and discussion

### 7.1 Stationary deformations

In Fig. 2 we show the stationary deformation correlations  $\langle \delta a_m^2 \rangle$ ,  $\langle \delta b_m^2 \rangle$  as a function of the mode number  $m$  for  $\Delta = 0.163$  and  $\chi \simeq 9.3$ . We also show a fit of these correlations for  $m \geq 3$  with the theoretical prediction (65). From the fit we can extract the tension  $\Sigma$ . In this particular example we obtain  $\Sigma_{\text{fit}} \simeq 103\kappa/R_0^2$ , whereas theory predicts  $\Sigma_{\text{theor}} \simeq 113\kappa/R_0^2$  from Eqs. (66)–(68).

The mean field treatment (65) predicts  $\langle \delta a_m^2 \rangle = \langle \delta b_m^2 \rangle$  for all  $m$ . We can see that this holds only for  $m \geq 3$ . As explained in Sec. 4.3, this is due to the fluctuations in the line tension. In the inset of Fig. 2, we compare  $\langle \delta a_2^2 \rangle$ ,  $\langle \delta b_2^2 \rangle$  with the low temperature expansion (88), with very good agreement.

### 7.2 Tension vs shear rate

Fig. 3 shows the extracted dimensionless tensions  $\Sigma_{\text{fit}} R_0^2/\kappa$  for different dimensionless shear rates  $0 \leq \chi \leq 10$  and for two different excess lengths  $\Delta = 0.163$  and  $\Delta = 0.340$ .

The agreement with the theoretical prediction from a numerical solution of Eqs. (66)–(68) is satisfactory. The fact that this function is nearly a straight line implies that the large-shear-rate approximation (14) is valid down to small shear rates. We find a crossover shear rate  $\chi_c$ , below which there are deviations from a linear behavior. Theoretically, Eq. (71) gives an order-of-magnitude estimate of  $\chi_c \simeq 3.09$  for  $\Delta = 0.163$  and  $\chi_c \simeq 0.99$  for  $\Delta = 0.340$ .

### 7.3 Autocorrelation function

In Fig. 4, the time autocorrelation function  $\langle a_3(t)a_3(0) \rangle$  is shown as a function of dimensionless time  $\dot{\gamma}t$ . The data follows the expected exponential decay (64) very well. From the amplitude  $\langle \delta a_3(0)\delta a_3(0) \rangle$  we can extract a tension  $\Sigma \simeq 65\kappa/R_0^2$ , while from the time constant we deduce  $\Sigma \simeq 44\kappa/R_0^2$ . Theory predicts  $\Sigma_{\text{theor}} \simeq 73\kappa/R_0^2$ . Given the rather noisy data, this agreement seems reasonable. For moderate shear rates the autocorrelation function has decayed before the oscillations implied by Eq. (64) become noticeable. Even for the large shear rate  $\chi \simeq 5.6$  used in Fig. 4, the oscillations are barely visible. For the same reason the build up of cross correlation  $\langle a(t)b(0) \rangle$  is hidden in the numerical noise.

### 7.4 Inclination angle

We compare the averaged inclination angle  $\langle \Theta \rangle$  for different reduced areas  $A^*$  with Eq. (78) in Fig. 5, valid in the quasi-circular limit. The agreement with simulation data is satisfactory, given the large error bars. The 2d Keller-Skalak theory, which is also shown in the plot, gives slightly better agreement.

In Fig. 6, we show the fluctuations of the inclination angle  $\langle \Delta\Theta^2 \rangle \equiv \langle \Theta^2 \rangle - \langle \Theta \rangle^2$  as a function of the shear rate. The theoretical scaling is given by Eq. (86), and is in excellent agreement for  $A^* = 0.85$  ( $\Delta \simeq 0.53$ ),  $A^* = 0.9$  ( $\Delta \simeq 0.34$ ), and  $A^* = 0.95$  ( $\Delta \simeq 0.163$ ). The scaling of the fluctuations of  $\Theta$  for  $A^*$  differs significantly for  $A^* = 0.7$  ( $\Delta \simeq 1.23$ ). In the deterministic case, a vesicle with such a low reduced area would tumble within the quasi-circular theory. This implies that the quasi-circular approximation works well for  $\Delta \leq 0.53$  (corresponding to  $A^* \geq 0.85$ ) in two dimensions.

### 7.5 Tank-treading frequency

Finally, we show the rescaled tank-treading frequency  $\omega_{\text{tt}}/\dot{\gamma}$  as a function of  $A^*$  in Fig. 7. Again, agreement with the 2d Keller-Skalak theory is quite good, while the quasi-circular theory neglects the effect of the vesicle shape on the flow and would predict  $\omega_{\text{tt}}^{\text{QC}}/\dot{\gamma} = 1/2$ , see Eq. (79).

## 8 Summary

We have studied the fluctuations and deformation of a 2d vesicle in shear flow at finite temperature. In the limit of

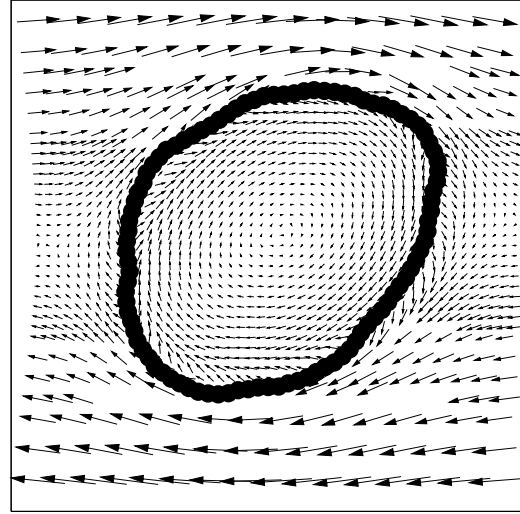


**Fig. 1.** Snapshot of the vesicle and the velocity field around it, taken from simulation data for reduced area  $A^* = 0.95$  and reduced shear rate  $\chi \simeq 5.6$  (see Eq. (39)). The disks represent the beads forming the membrane and are plotted to scale.

small deformations from a circle, we have derived analytical Langevin-type equations of motion, which are nonlinear due to the length constraint. A mean-field treatment allows approximate predictions for the stationary correlation functions and time autocorrelation functions of the deformation amplitudes, which agree quantitatively with simulation data. Deviations of the stationary correlations from the mean-field predictions in the lowest mode are explained quantitatively in a low temperature expansion of the original constrained Langevin equations. The mean inclination angle and the tank-treading frequency are better described by a deterministic 2d Keller-Skalak theory. Fluctuations of the inclination angle are also determined quantitatively. Theory and simulations agree well for low excess lengths, but differ for larger excess lengths.

The good quantitative agreement of mesoscale simulations of vesicles in flow with detailed theoretical calculations demonstrates the predictive power of these simulation methods for more complex flow geometries.

RF, US and GG would like to acknowledge financial support through the DFG priority program SPP 1146 “Micro- and Nanofluidics”. AL and GG acknowledge fruitful discussions with H. Noguchi, M. Ripoll, G. Vliгентhart, and R. Winkler. AL thanks Gerhard Gompper and co-workers for hospitality at the Forschungszentrum Jülich and acknowledges support from CNR through the Short-Term Mobility Program.

## References

1. M. Kraus, W. Wintz, U. Seifert, and R. Lipowsky, *Phys. Rev. Lett.* **77**, 3685 (1996).
2. T. Biben and C. Misbah, *Phys. Rev. E* **67**, 031908 (2003).

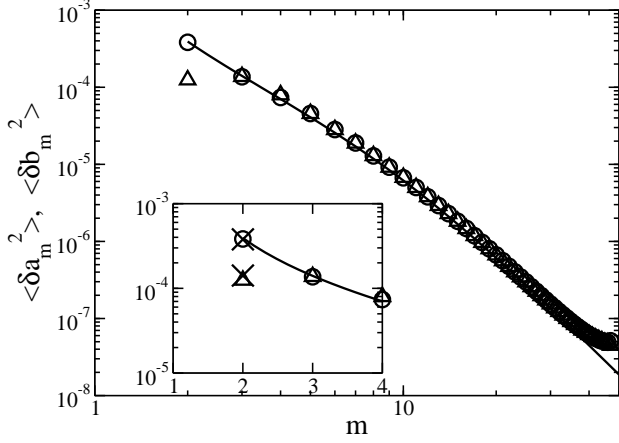


**Fig. 2.** Stationary correlations  $\langle \delta a_m^2 \rangle$  (triangles) and  $\langle \delta b_m^2 \rangle$  (circles) as a function of mode number  $m$  on a double logarithmic scale. The solid line corresponds to a fit of Eq. (65) with  $\Sigma_{\text{fit}} \simeq 103\kappa/R_0^2$ . The inset highlights  $\langle \delta a_2^2 \rangle$ ,  $\langle \delta b_2^2 \rangle$  in comparison with the low-temperature expansion Eq. (88) (crosses). Simulation parameters are  $\Delta = 0.163$  (corresponding to  $A^* = 0.95$ ) and  $\chi \simeq 9.3$ .

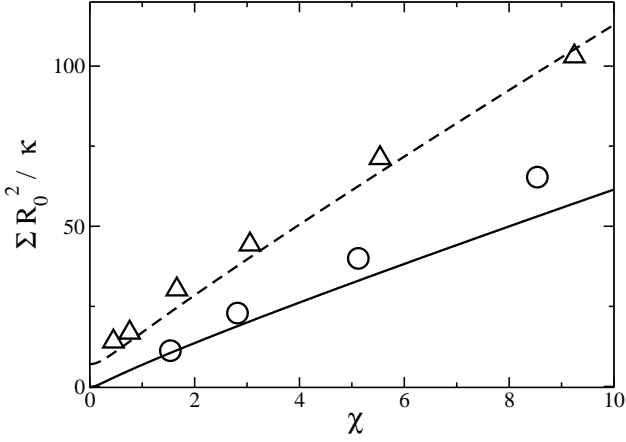


**Fig. 3.** Dimensionless tension  $\Sigma R_0^2 / \kappa$  as a function of reduced shear rate  $\chi$ . Symbols denote the fitted tensions  $\sigma_{\text{fit}}$  extracted from fluctuation spectra for excess lengths  $\Delta = 0.163$  (triangles) and  $\Delta = 0.340$  (circles), corresponding to  $A^* = 0.95$  and  $A^* = 0.9$ , respectively (compare Fig. 2). The solid and dashed lines show the corresponding numerical solution of Eqs. (66)–(68).

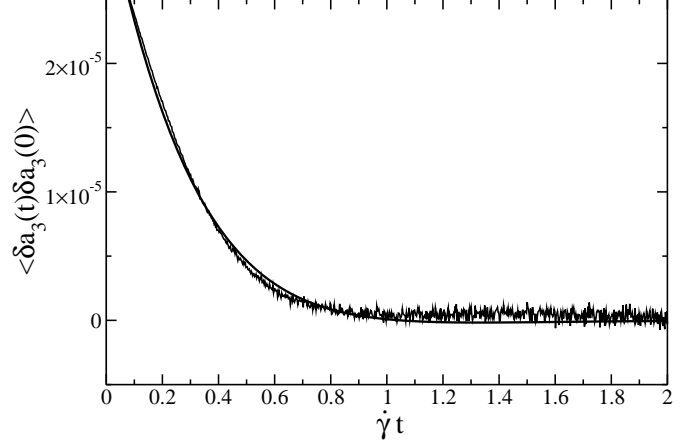


**Fig. 4.** Autocorrelation function  $\langle \delta a_3(t) \delta a_3(0) \rangle$  of the  $a_3$  mode as a function of dimensionless time  $\dot{\gamma}t$ . Simulation parameters are  $\Delta = 0.163$ ,  $\chi = 5.6$ . The solid line shows a fit of Eq. (64).

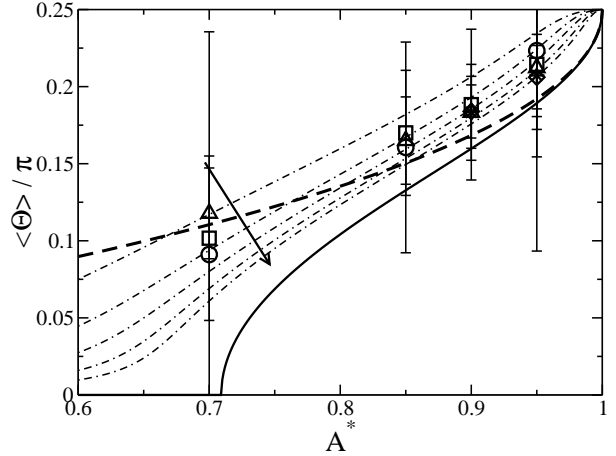


**Fig. 5.** Scaled average inclination angle  $\langle \Theta \rangle / \pi$  as a function of reduced area  $A^*$ . Symbols with error bars show simulation data for different values of the reduced shear rate  $\chi = 10.0A^{*3/2}$  (diamonds),  $\chi = 6.0A^{*3/2}$  (stars),  $\chi = 3.3A^{*3/2}$  (triangles),  $\chi = 1.8A^{*3/2}$  (squares),  $\chi = 0.8A^{*3/2}$  (circles). The continuous line corresponds to the deterministic limit Eq. (78) and is independent of  $\chi$ . Dashed-dot lines follow from the mean-field Eq. (53) with  $\chi A^{*3/2} \in \{0.8, 1.8, 3.3, 6, 10\}$  growing in the direction indicated by the arrow. The thick dashed line follows from the Keller-Skalak theory, see Eq. (96).

3. J. Beaucourt, F. Rioual, T. Seon, T. Biben, and C. Misbah, Phys. Rev. E **69**, 011906 (2004).
4. F. Rioual, T. Biben, and C. Misbah, Phys. Rev. E **69**, 061914 (2004).
5. H. Noguchi and G. Gompper, Phys. Rev. Lett. **93**, 258102 (2004).
6. H. Noguchi and G. Gompper, Phys. Rev. E **72**, 011901 (2005).

7. P. M. Vlahovska and R. S. Gracia, Phys. Rev. E **75**, 016313 (2007).
8. K. de Haas, C. Blom, D. van den Ende, M. H. G. Duits, and J. Mellema, Phys. Rev. E **56**, 7132 (1997).
9. V. Kantsler and V. Steinberg, Phys. Rev. Lett. **95**, 258101 (2005).
10. B. Lorz, R. Simson, J. Nardi, and E. Sackmann, Europhys. Lett. **51**, 468 (2000).

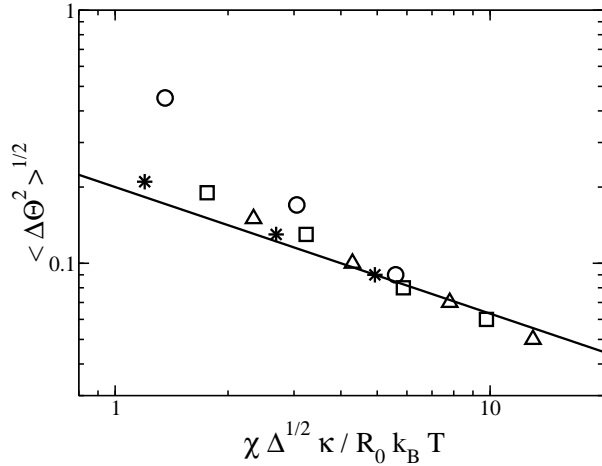


**Fig. 6.** Fluctuations of the inclination angle  $\langle \Delta\Theta^2 \rangle^{1/2}$  as a function of reduced shear rate  $\chi \Delta^{1/2} \kappa / (R_0 k_B T)$ . Symbols denote simulation data for different  $A^* = 0.95$  (squares),  $A^* = 0.90$  (triangles),  $A^* = 0.85$  (stars),  $A^* = 0.7$  (circles), corresponding to  $\Delta \simeq 0.163$ ,  $\Delta \simeq 0.34$ ,  $\Delta \simeq 0.53$ , and  $\Delta \simeq 1.23$ , respectively. The solid line is the quasi-circular scaling prediction of Eq. (86).

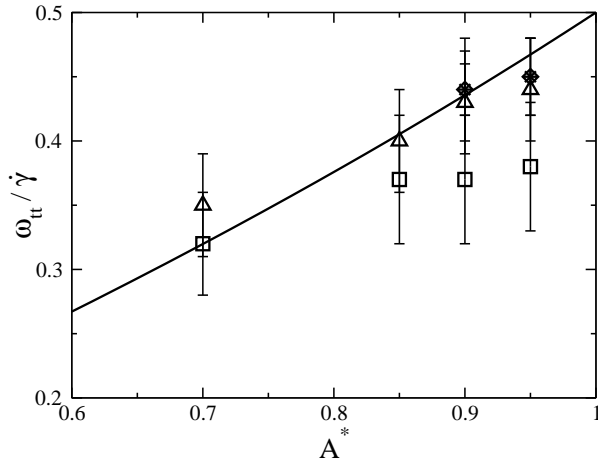


**Fig. 7.** Tank-treading frequency  $\omega_{tt}$  rescaled by shear rate  $\dot{\gamma}$ , as a function of reduced area  $A^*$  for different values of the reduced shear rate  $\chi = 10.0A^{*3/2}$  (diamonds),  $6.0A^{*3/2}$  (stars),  $3.3A^{*3/2}$  (triangles),  $1.8A^{*3/2}$  (squares). The solid line follows from the Keller-Skalak theory, see Eq. (93).

11. M. Abkarian, C. Lartigue, and A. Viallat, Phys. Rev. Lett. **88**, 068103 (2002).  
 12. U. Seifert, Phys. Rev. Lett. **83**, 876 (1999).  
 13. I. Cantat and C. Misbah, Phys. Rev. Lett. **83**, 880 (1999).  
 14. S. Sukumaran and U. Seifert, Phys. Rev. E **64**, 11916 (2001).  
 15. J. Beaucourt, T. Biben, and C. Misbah, Europhys. Lett. **67**, 676 (2004).

16. V. Kantsler and V. Steinberg, Phys. Rev. Lett. **96**, 36001 (2006).  
 17. C. Misbah, Phys. Rev. Lett. **96**, 28104 (2006).  
 18. H. Noguchi and G. Gompper, Phys. Rev. Lett. **98**, 128103 (2007).  
 19. V. V. Lebedev, K. S. Turitsyn, and S. S. Vergeles, arXiv:cond-mat/0702650v1 (2007).  
 20. G. Danker, T. Biben, T. Podgorski, C. Verdier, and C. Misbah, arXiv:cond-mat/0703698v2 (2007).  
 21. U. Seifert, Eur. Phys. J. B **8**, 405 (1999).  
 22. A. Malevanets and R. Kapral, J. Chem. Phys. **110**, 8605 (1999).  
 23. A. Malevanets and R. Kapral, J. Chem. Phys. **112**, 7260 (2000).  
 24. N. Kikuchi, C. M. Pooley, J. F. Ryder, and J. M. Yeomans, J. Chem. Phys. **119**, 6388 (2003).  
 25. J. M. Yeomans, Physica A **369**, 159 (2006).  
 26. A. Lamura, G. Gompper, T. Ihle, and D. M. Kroll, Europhys. Lett. **56**, 319 (2001).  
 27. A. Lamura and G. Gompper, Eur. Phys. J. E **9**, 477 (2002).  
 28. N. Kikuchi, J. F. Ryder, C. M. Pooley, and J. M. Yeomans, Phys. Rev. E **71**, 061804 (2005).  
 29. M. Ripoll, R. G. Winkler, and G. Gompper, Phys. Rev. Lett. **96**, 188302 (2006).  
 30. H. Noguchi and G. Gompper, Proc. Natl. Acad. Sci. USA **102**, 14159 (2005).  
 31. S. R. Keller and R. Skalak, J. Fluid. Mech. **120**, 27 (1982).  
 32. M. do Carmo, *Differential Geometry of Curves and Surfaces* (Englewood Cliffs, NJ: Prentice Hall, 1976).  
 33. W. Helfrich, Z. Naturf. C **28**, 693 (1973).  
 34. O. Kratky and G. Porod, Rec. Trav. Chim. **68**, 1106 (1949).  
 35. L. D. Landau and E. M. Lifshitz, *Fluid mechanics*, vol. 6 (London, Pergamon Press, 1959).  
 36. J. Happel and H. Brenner, *Low Reynolds number hydrodynamics* (The Hague, Martinus Nijhoff Publishers, 1983).  
 37. G. B. Jeffery, P. Roy. Soc. A **102**, 161 (1922).  
 38. M. Ripoll, K. Mussawisade, R. G. Winkler, and G. Gompper, Europhys. Lett. **68**, 106 (2004).  
 39. T. Ihle and D. M. Kroll, Phys. Rev. E **63**, 020201(R) (2001).  
 40. T. Ihle, E. Tüzel, and D. M. Kroll, Phys. Rev. E **70**, 035701(R) (2004).